Article

Efficient Amplitude-Modulated Pulses for Triple- to Single-Quantum Coherence Conversion in MQMAS NMR

Henri Colaux, Daniel M. Dawson, and Sharon E. Ashbrook*

School of Chemistry, EaStCHEM and Centre for Magnetic Resonance, University of St. Andrews, North Haugh, St. Andrews KY16 9ST, U.K.

ⓢ *Supporting Information*

ABSTRACT: The conversion between multiple- and single-quantum coherences is integral to many nuclear magnetic resonance (NMR) experiments of quadrupolar nuclei. This conversion is relatively inefficient when effected by a single pulse, and many composite pulse schemes have been developed to improve this efficiency. To provide the maximum improvement, such schemes typically require time-consuming experimental optimization. Here, we demonstrate an approach for generating amplitude-modulated pulses to enhance the efficiency of the triple- to single-quantum conversion. The optimization is performed using the SIMPSON and MATLAB packages and results in efficient pulses that can be used without experimental reoptimisation. Most significant signal enhancements are obtained when good estimates of the inherent radio-frequency nutation rate and the magnitude of the quadrupolar coupling are used as input to the optimization, but the pulses appear robust to reasonable variations in either parameter, producing significant enhancements compared to a single-pulse conversion, and also comparable or improved efficiency over other commonly used approaches. In all cases, the ease of implementation of our method is advantageous, particularly for cases with low sensitivity, where the improvement is most needed (e.g., low gyromagnetic ratio or high quadrupolar coupling). Our approach offers the potential to routinely improve the sensitivity of high-resolution NMR spectra of nuclei and systems that would, perhaps, otherwise be deemed "too challenging".
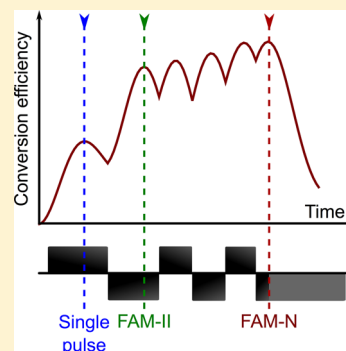
■ INTRODUCTION

Although nuclear magnetic resonance (NMR) spectroscopy offers a sensitive probe of the atomic-scale environment, in the solid state the presence of anisotropic interactions hinders the extraction of accurate structural information.[1] For nuclei with spin quantum number $I = 1/2$, magic-angle spinning (MAS),[2] i.e., rapid rotation of the sample around an axis inclined at 54.736° to the external magnetic field, B_0, is able to remove the anisotropic broadening and produce high-resolution spectra, providing the rotation rate is sufficiently rapid. However, for quadrupolar nuclei, with $I > 1/2$, MAS is not able to completely remove the second-quadrupolar broadening, no matter how fast the sample is rotated.[3] For quadrupolar nuclei with half-integer spin quantum number, a variety of approaches have been introduced to remove the quadrupolar interaction completely and acquire high-resolution spectra. Early methods involved sample rotation around two different axes; simultaneously in the double rotation (DOR)[3,4] experiment, and sequentially for dynamic angle spinning (DAS).[3,5] Though successful, these methods require expensive and specialist hardware and, particularly for DOR, spinning rates can be somewhat limited in comparison to simple MAS.

NMR study of quadrupolar nuclei in solids was revolutionized by the introduction of the multiple-quantum (MQ) MAS experiment by Frydman and Harwood in 1995,[6] as this offered the possibility of acquiring high-resolution spectra using purely conventional MAS hardware. This two-dimensional experiment (acquired under MAS conditions) involves the correlation of multiple-quantum coherences (usually triple-quantum, i.e., $m_I = +3/2 \leftrightarrow m_I = -3/2$) with central-transition (i.e., $m_I = +1/2 \leftrightarrow m_I = -1/2$) coherences. This approach has gained widespread popularity and has been applied to the study of ceramics, minerals, microporous materials, energy materials, and glasses.[3,7] More recently, Gan introduced the satellite-transition (ST) MAS experiment,[8] which is conceptually similar to MQMAS but correlates the single-quantum satellite (i.e., $m_I = \pm1/2 \leftrightarrow m_I = \pm3/2$) and central transitions. Despite offering a sensitivity advantage over MQMAS, this experiment is technically more challenging to implement (owing to the need to accurately set the angle of the spinning axis, and the requirement for a very stable spinning rate)[8,9] and has received less attention, although it has been utilized very successfully in cases where sensitivity is limited, and to detect the presence of μs-time scale dynamics.[3,8,10]

Despite its extensive use, MQMAS does suffer from inherently poor sensitivity, owing to the need for filtration through multiple-quantum coherences. This is a particular problem if significant quadrupolar broadening is present, or for cases where only low radio-frequency (rf) field strength is available. Several methods have been developed to improve the

efficiency of MQMAS, with particular attention focused on the "conversion" pulse, i.e., the conversion of triple- to single-quantum coherences, as shown in Figure 1. DFS (double
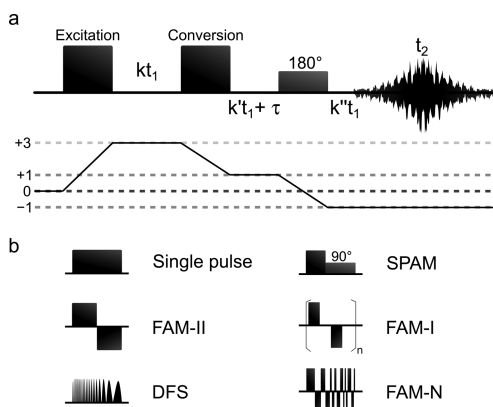

Figure 1. Pulse sequence and coherence transfer pathway diagram for a phase-modulated split-t_1 shifted-echo triple-quantum MAS experiment. The conversion of triple- to single-quantum coherences can be carried out using a range of different types of pulses as shown. For the ^{87}Rb experiments performed in this work $k = 9/16$, $k' = 7/16$, and $k'' = 0$. The final pulse in the sequence (and the additional pulse for SPAM) is chosen to be selective for the central transition.

frequency sweep),[11] FAM (fast amplitude modulated),[12,13] SPAM (soft pulse added mixing,)[14,15] and HS (hyperbolic secant)[16] pulses have all been shown to yield improved efficiency over the use of a single high-power pulse for this coherence transfer. Although significant sensitivity gains are possible, achieving these in practice becomes more difficult as the complexity of the pulses used increases. SPAM offers a very simple approach to increased sensitivity (involving the addition of a central-transition selective 90° pulse after the high-power conversion pulse) and is therefore easy to optimize and to implement.[14,15,17] More significant improvements can often be obtained using FAM pulses, which consist of a number of independent oppositely phased high-power pulses, that can be applied in a "windowed" (FAM-I)[12] or "windowless" (FAM-II)[13] manner. In the latter case, the number of pulses applied is often restricted to two, leading also to a reasonably straightforward experimental optimization process. However, it has been demonstrated that in some cases better sensitivity can be achieved by using a larger number of pulses, all of which vary in duration.[13,18] However, this significantly increases the difficulty of the experimental multidimensional optimization, particularly for cases where sensitivity is limiting. The DFS approach introduced by Kentgens and Verhagen can produce impressive gains in sensitivity but can be more challenging to optimize in practice than some of the simpler approaches.[11,19]

Although the experimental optimization of composite pulses can be practically challenging, and certainly very time-consuming, particularly for the very cases where the sensitivity enhancement they provide is vital for achieving high-resolution spectra on a reasonable time scale, two previous attempts (both using numerical simulations rather than a more laborious experimental route) have been made to improve the efficiency of pulses based on FAM-II.[13,18] In the approach of Goldbourt et al.,[13] the length of the initial pulse was varied until a maximum in conversion efficiency was reached, at which point a second pulse was added with opposite phase. The length of this pulse was increased (from zero) until a maximum in

conversion efficiency was reached, and then a third pulse of opposite phase was added. This approach was continued with up to four oppositely phased pulses used in the original work and with an enhancement factor of ∼3 (200% more signal) reported, relative to the most efficient single-pulse conversion. In the approach of Morais et al.,[18] it was noted that when sequential oppositely phased pulses are used, for spin $I = 3/2$, the optimum length of the first pulse corresponded to an inherent flip angle of 90°, i.e., the point of the echo/antiecho crossing, and this value was used as a constraint. Though the precise details of the remainder of the optimization procedure are somewhat unclear from the original work, composite pulses were generated, composed of up to six oppositely phased pulses, and yielding signal enhancement factors slightly higher than those obtained by Goldbourt et al.[13] One possible reason for the improved efficiency of the optimized pulses of Morais et al., relative to those of Goldbourt et al., is the removal of the constraint that the phase must be inverted only when a maximum in signal is obtained. Morais et al. demonstrated that, by increasing the length of the preceding pulse beyond this point, greater overall efficiency could be achieved by the following pulse. It is interesting to note that the pulses developed by Morais et al. appear to be essentially invariant with both the rf nutation frequency and the magnitude of the quadrupolar coupling, suggesting that they may have essentially universal applicability (at least under the conditions considered). However, the optimization procedure of Morais et al. still appears to have been constrained so that each pulse is shorter than the preceding one. In this work, we also exploit the fast and efficient optimization offered by high-throughput computer simulation using modern hardware to develop a series of composite FAM-II pulses, where additional oppositely phased pulses continue to be added until no additional gain in sensitivity is observed. However, as described in the procedure below, there is no constraint on the relative lengths or efficiencies of the individual pulses, but instead, the pulse durations are optimized to obtain the overall maximum efficiency. We demonstrate that these composite pulses, termed here FAM-N (with N denoting the number of oppositely phased pulses in the composite pulse), are easy and quick to produce, provide improved sensitivity over conventional FAM-II in most cases, require little or no experimental reoptimization and appear robust with respect to reasonable variation of the experimental parameters. This appears to offer a very promising approach for routine implementation and sensitivity enhancement of MQMAS experiments.

■ EXPERIMENTAL AND COMPUTATIONAL DETAIL

Computer Simulation and Optimization. High-throughput computer optimization was performed using the SIMPSON density matrix simulation program,[20] which was called from a home-written MATLAB[21] script (see Supporting Information for more detail). Specified within the optimization are the external magnetic field strength, the MAS rate, the inherent radio-frequency nutation rate, and the quadrupolar parameters (i.e., the magnitude of the quadrupolar coupling, $C_Q = eQV_{zz}/h$, and the asymmetry parameter, $\eta_Q = (V_{xx} - V_{yy})/V_{zz}$, where V_{ii} are the principal components of the electric field gradient tensor in its principal axis system, and eQ is the nuclear quadrupole moment).[3] The transfer of a unit amount of triple-quantum coherences (density matrix element 1, 4 for $I = 3/2$) to central-transition single-quantum coherences of the same sign (density matrix element 2, 3 for $I = 3/2$) is considered.

Once optimum efficiency has been achieved, the composite pulse that produces this is saved to a text file and can also be written directly into a triple-quantum filtered and/or a two-dimensional triple-quantum MAS pulse program.

The computer-based optimization procedure used is shown schematically in Figure 2. This can be broken down into a number of key steps. See Supporting Information for a more detailed description.
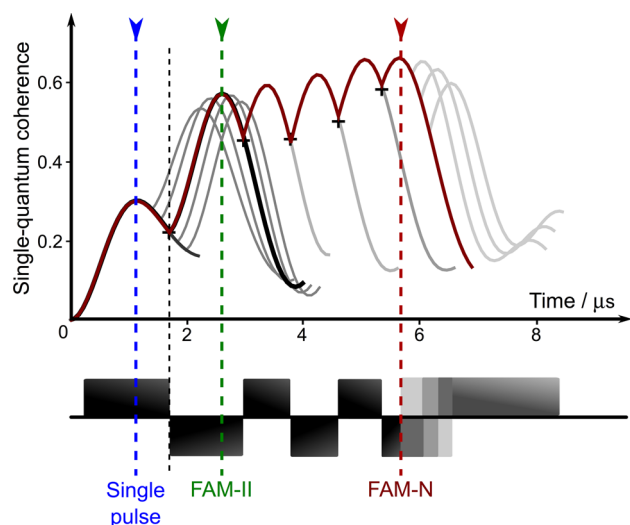

Figure 2. Schematic description of the computational optimization process for the generation of FAM-N pulses. Simulations have been performed for ^{87}Rb ($I = 3/2$) at $B_0 = 14.1$ T with $\omega_1/2\pi = 150$ kHz, $\omega_R/2\pi = 12.5$ kHz, $C_Q = 1.2$ MHz, and $\eta_Q = 0$. The plot shows the amount of central-transition single-quantum coherence generated from a unit amount of triple-quantum coherence as a function of the duration of the pulse(s). Highlighted are the duration (and maximum efficiency) of a single pulse (blue dotted line), FAM-II (green dotted line), and FAM-N (red dotted line). For the case shown, the optimum FAM-N pulse has six consecutive pulses of opposite phase.

Step 1: The amount of central-transition single-quantum coherence generated in the simulation from unit triple-quantum coherence of the same sign is monitored as the duration of a high-power rf pulse is varied. The point at which maximum conversion is obtained (for one pulse) is highlighted in Figure 2 by the blue dotted line.

Step 2: The duration of the first pulse is chosen to be that producing the maximum coherence transfer, and a second pulse is then applied with an inverted phase. The duration of this pulse is incrementally varied. The duration of the previous pulse is then increased by one increment and the variation of the second pulse is repeated. This procedure is carried out a number of times until additional incrementation of the first pulse would result in a decrease in the maximum transfer achieved. At this point an additional pulse is added, again with inverted phase.

Step 3: This procedure is repeated, i.e., incrementing the duration of the $(N − 1)$th pulse, and varying the duration of the Nth pulse for each increment and determining the point of maximum coherence transfer. This generates a series of pulses with opposite phase and varying duration. As described in the Supporting Information, changing the lengths of pulses preceding the $(N − 1)$th pulse does not lead to any further enhancement and is omitted from the procedure for increased time efficiency.

Step 4: The optimization is stopped when adding the next pulse does not result in an increase in the maximum conversion efficiency at any point.

Step 5: The optimum composite pulse train produced is saved to a text file, listing the duration of each step and the coherence transfer efficiency throughout. The pulse can also be written directly into an experimental NMR pulse program. The pulse is usually defined by its total length and the relative duration of each alternately phased step. The total pulse duration can then also be experimentally optimized if desired or, perhaps more usefully, the applied B_1 field strength (i.e., the inherent rf nutation rate) can be varied.

As an example, Figure 2 shows the amount of central-transition single-quantum coherence generated from initial triple-quantum coherence as a function of the duration of high-power pulses ($\omega_1/2\pi = 150$ kHz), for a ^{87}Rb ($I = 3/2$) nucleus with $C_Q = 1.2$ MHz, $\eta_Q = 0$, and $B_0 = 14.1$ T (600 MHz spectrometer), with an MAS rate, $\omega_R/2\pi$, of 12.5 kHz. For a single pulse, maximum conversion is achieved with a duration of 1.18 μs (see the blue dotted line in Figure 2). However, if a second pulse is added with alternate phase, an increase in conversion efficiency is immediately apparent. When the length of the initial pulse is increased and the variation of the duration of the second pulse repeated, maximum coherence transfer is observed with p1 = 1.78 μs and p2 = 0.88 μs. This would correspond to a conventional FAM-II pulse, as indicated by the green dotted line in Figure 2. This procedure can be repeated and an additional sensitivity gain is observed with a longer pulse train (e.g., of 120% over a single pulse and 16% over FAM-II, with $N = 6$). The pulses generated by this optimization differ from both the pulses of Goldbourt et al.,[13] where the length of the first pulse would be constrained to 1.18 μs (i.e., the value giving the most efficient single-pulse conversion) and the pulses of Morais et al.,[18] where the length of the first pulse would be constrained to 1.67 μs (i.e., an inherent 90° pulse). Further comparison of the pulses obtained by the three different optimization methods is provided in the Supporting Information. The computer-based optimization is easy to implement (as this is controlled automatically by the MATLAB routine) and is cost efficient to carry out (unlike its experimental counterpart). If necessary, optimization can be implemented in a high-throughput approach, varying the quadrupolar parameters, rf nutation rate or MAS rate in a series of sequential optimizations.

NMR Spectroscopy. Experimental NMR spectra were acquired at room temperature using a Bruker Avance III 600 MHz spectrometer equipped with a 14.1 T wide-bore magnet, at a Larmor frequency of 196.4 MHz for ^{87}Rb. Samples were packed into conventional 4 mm rotors and rotated at MAS rates, $\omega_R/2\pi$, of 12.5 kHz in a commercial 4 mm MAS probe, with inherent rf nutation rates, $\omega_1/2\pi$, between 110 and 125 kHz (calibrated using RbCl). Central-transition selective pulses were applied with typical rf nutation rate, $\omega_1/2\pi$, of ∼8 kHz. Chemical shift scales are shown in ppm, referenced relative to RbNO$_{3(aq)}$ (using RbCl at 128 ppm as a secondary reference).[22] Triple-quantum filtered experiments were performed using a phase-modulated two-pulse sequence, using a high-power excitation pulse, and conversion of triple- to single-quantum coherences achieved using (i) a single high-power pulse, (ii) SPAM, (iii) FAM-I, (iv) FAM-II, (v) DFS, or (vi) FAM-N pulses. For (i)−(v) these pulses were experimentally optimized until the maximum signal was achieved. Generation and optimization of FAM-N pulses are described in detail in the

6020

dx.doi.org/10.1021/jp505752c | J. Phys. Chem. A 2014, 118, 6018−6025

text. Two-dimensional triple-quantum MAS experiments were recorded using a phase-modulated split-t_1 shifted-echo pulse sequence,[23] with selection of the $+3 \rightarrow +1 \rightarrow -1$ coherence transfer pathway, as shown in Figure 1. The conversion of triple- to single-quantum coherences was achieved using methods (i)−(vi), as described above. The third pulse is a central-transition selective inversion pulse. The indirect dimension is referenced according to the convention described in ref 24. See Supporting Information for more details for specific experiments.

RESULTS AND DISCUSSION

Figure 3a compares the maximum single-quantum coherence generated (in a simulation) from unit triple-quantum coherence
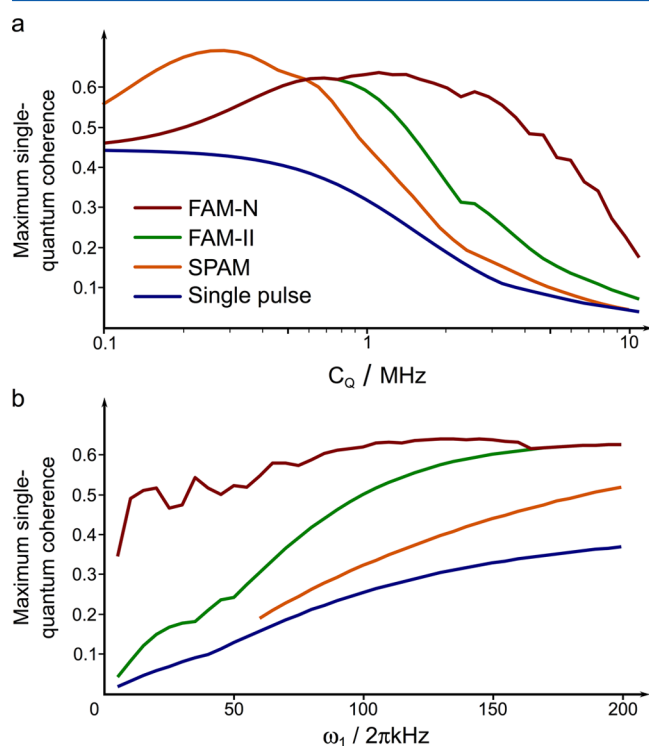

Figure 3. Plots of the maximum central-transition single-quantum coherence generated from unit triple-quantum coherence using an optimized single pulse (blue line), SPAM (orange line), FAM-II (green line), or FAM-N (red line) pulses as a function of (a) the quadrupolar coupling constant, C_Q, and (b) the inherent rf nutation rate, $\omega_1/2\pi$. Simulations were performed for a single ^{87}Rb ($I = 3/2$) nucleus at $B_0 = 14.1$ T, with $\eta_Q = 0$, $\omega_R/2\pi = 12.5$ kHz, and (a) $\omega_1/2\pi = 114$ kHz or (b) $C_Q = 1.2$ MHz. For SPAM, the optimization program was limited to two pulses, with the second having $\omega_1/2\pi = 10$ kHz.

for some of the different types of conversion pulses, as a function of the quadrupolar coupling constant (C_Q). The simulation was carried out for a single ^{87}Rb ($I = 3/2$) nucleus with $\eta_Q = 0$, at $B_0 = 14.1$ T, subject to a pulse with $\omega_1/2\pi = 114$ kHz and with $\omega_R/2\pi = 12.5$ kHz. The conversion efficiency for a single pulse and for FAM-II is easy to obtain from the FAM-N optimization process (as shown in Figure 2). To simulate a SPAM conversion pulse, the program described above was limited to just two pulses, the second of which was set to have a much lower rf nutation rate (∼10 kHz in this simulation). It is clear from Figure 3a that the efficiency of a single high-power pulse for the conversion of triple- to single-quantum

coherences decreases significantly as the quadrupolar coupling increases. The efficiency of SPAM is greater than that of a single pulse for all values of C_Q considered, with maximum efficiency observed when C_Q is ∼0.3 MHz. For a FAM-II conversion pulse (with two pulses) maximum efficiency is achieved at higher C_Q values (∼0.7 MHz). Although the efficiency of FAM-II decreases at higher values of the quadrupolar interaction, it is more efficient then either SPAM or a single pulse above ∼1 MHz, but less efficient than SPAM at lower C_Q. The FAM-N pulse has the highest efficiency of the methods considered here at higher values of C_Q, with significant improvements over a single pulse for values above 1 MHz. Note that the efficiencies of FAM-N and FAM-II are identical below ∼0.9 MHz, as in this regime it is found that $N = 2$, i.e., that FAM-II is the most efficient FAM-type pulse at low C_Q values. Figure 3b shows a similar plot of conversion efficiency, but with C_Q now fixed at 1.2 MHz and the rf nutation rate varied. The conversion efficiency using a single pulse increases as the rf nutation rate increases, and similar behaviors are also observed for both SPAM and FAM-II. FAM-II exhibits an enhancement of a factor of ∼2 over that achieved with a single pulse for most of the parameter space considered. The conversion efficiency obtained using FAM-N is the highest observed at each of the rf values considered, and remains fairly constant, rising slightly as the nutation rate increases. Note that at high values of the nutation rate the FAM-N and FAM-II pulses are formally identical.

Figure 4a shows a ^{87}Rb MAS spectrum of RbNO$_3$, where the quadrupolar line shapes of the three distinct Rb sites (all of which exhibit similar C_Q values, between 1.65 and 2.0 MHz),[25] are overlapped. Three distinct resonances can be seen in the isotropic projections shown in Figure 4b, obtained from ^{87}Rb
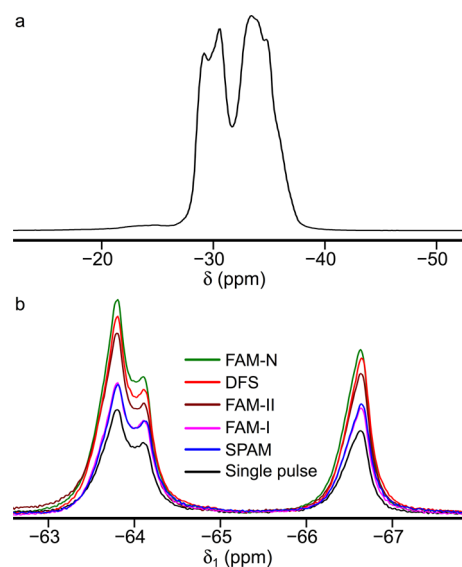

Figure 4. ^{87}Rb (14.1 T, 12.5 kHz) (a) MAS and (b) isotropic projections of triple-quantum MAS NMR spectra of RbNO$_3$. In (b), spectra were acquired using the pulse sequence in Figure 1, with different pulses for the conversion of triple- to single-quantum coherences. The single pulse, SPAM, FAM-I, FAM-II, and DFS pulses were optimized experimentally (Supporting Information). The FAM-N pulse was generated for a single ^{87}Rb spin at 14.1 T with $\omega_1/2\pi = 114$ kHz, $\omega_R/2\pi = 12.5$ kHz, $C_Q = 1.9$ MHz, and $\eta_Q = 0$. For full details of the experimental parameters used, see the Supporting Information.

two-dimensional triple-quantum MAS NMR experiments, acquired using the phase-modulated split-t_1 shifted-echo pulse sequence shown in Figure 1. The conversion of single- to triple-quantum coherences was carried out using different approaches in the six different spectra shown. The single pulse, SPAM, FAM-I, FAM-II, and DFS pulses were optimized experimentally (resulting in the pulses described in the Supporting Information). For FAM-N, the pulse was produced using the computational optimization approach described above, using $\omega_1/2\pi$ = 114 kHz, $\omega_R/2\pi$ = 12.5 kHz, C_Q = 1.9 MHz, and η_Q = 0. It is possible to perform an additional experimental optimization step by varying the B_1 field strength to ensure maximum signal is obtained (e.g., to account for any inaccuracies in estimation or calibration of the rf nutation rate). In this particular case experimental optimization did not result in any improvement. Figure 4 shows that for all three sites FAM-N has much greater efficiency than the single-pulse conversion (∼105% more signal) and greater also than FAM-II (by ∼20%). The efficiency is slightly higher than that achieved using DFS, although it is not clear whether this result arises from the more challenging experimental optimization for DFS or from an inherent difference in efficiency. Both FAM-N and SPAM require little or no experimental reoptimization, ensuring they are easy to implement. The additional optimization time required increases for FAM-II, FAM-I, and DFS experiments, respectively.

Although similar sensitivity enhancements were observed using FAM-N for all Rb sites in RbNO$_3$, all three do have similar C_Q values. However, the value of η_Q differs significantly between the three. Figure 5 plots how the (simulated)

Table 1. Amount of [87]Rb Central-Transition Single-Quantum Coherence Generated from Unit Triple-Quantum Coherence Using a Single Pulse or Different FAM-N Pulses for Species with C_Q and η_Q Values Shown (Simulation Parameters: B_0 = 14.1 T, $\omega_1/2\pi$ = 114 kHz, and $\omega_R/2\pi$ = 12.5 kHz, with C_Q and η_Q as Shown)

site	C_Q/ MHz	η_Q	single-quantum coherence			
			single pulse	FAM-N $(1.9, 0)^a$	FAM-N $(C_Q, 0)^b$	FAM-N $(C_Q, \eta_Q)^c$
	1.9	0	0.190	0.581		
Rb1	1.68	0.2	0.213	0.544	0.573	0.593
Rb2	1.94	1	0.179	0.495	0.502	0.546
Rb3	1.72	0.5	0.206	0.497	0.530	0.585

^{a}FAM-N pulse generated using C_Q = 1.9 MHz and η_Q = 0. ^{b}FAM-N pulse generated using C_Q values specific to each site and η_Q = 0. ^{c}FAM-N pulse generated using C_Q and η_Q values specific to each site.

using a single pulse) when applied in simulation to sites with C_Q and η_Q values for the three Rb species in RbNO$_3$. For a species with C_Q = 1.9 MHz and η_Q = 0 the FAM-N pulse generated using these NMR parameters gives 306% of the signal of that using a single pulse (i.e., a 206% enhancement). When this same pulse is applied at the C_Q/η_Q values found for the three Rb sites in RbNO$_3$, a decrease in efficiency is found (with enhancements between 155 and 177% obtained). The signal obtained increases in all cases when the FAM-N pulse applied has been generated for the specific C_Q values for each site and increases further still when the pulse applied is generated initially using both C_Q and η_Q values. However, in all cases, significant signal enhancements over a single pulse are obtained.

The FAM-N computer-based optimization requires initial input of the rf nutation rate, the MAS rate, and C_Q (and η_Q). Although the MAS rate is easily set experimentally, it may well be that the rf nutation rate is not known exactly, or that C_Q values may not be accurately known (or may vary between different sites within the same sample). The latter point, of course, presents a challenge for any signal enhancement technique (and indeed MQMAS itself is famously non-quantitative as a function of C_Q); however, the need to know ω_1 and C_Q in advance could be seen as an additional challenge or requirement for the FAM-N approach. It is generally relatively easy to measure (or at least estimate) the inherent rf nutation rate using a sample where C_Q = 0. There are a number of options for estimating C_Q values if rf nutation rates are not known exactly, either from a comparison to similar materials in the literature, using first-principles calculations if a structural model is available, or from the MAS spectrum. Although in the latter case it may not be possible to extract very accurate values if the spectrum consists of a number of overlapping line shapes, estimates can often be obtained and, in the worst cases, an upper limit determined from the line width.

Despite the options outlined above, it is instructive to consider how the efficiency of FAM-N varies if the pulses are applied under different conditions to those for which they were initially optimized (i.e., to investigate the robustness of the method to variation in experimental or sample parameters). Figure 6a plots how the efficiency of a specific FAM-N pulse (optimized at the inherent rf nutation rate shown) varies as the nutation rate at which the sequence is carried out changes. For example, the bright red line shows how the (simulated) efficiency of a FAM-N pulse optimized using $\omega_1/2\pi$ = 100 kHz,
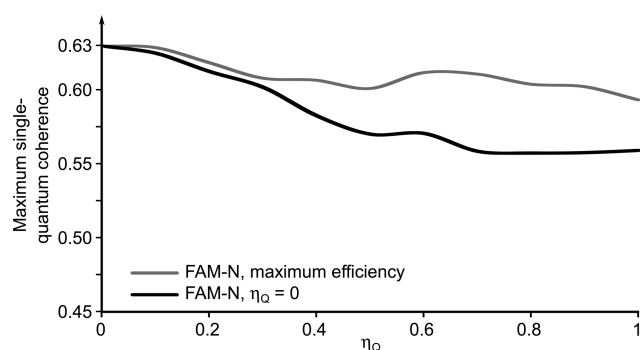

Figure 5. Plot of the variation in the maximum central-transition single-quantum coherence obtained from unit triple-quantum coherence using a FAM-N pulse as a function of η_Q. Results are shown either for a FAM-N pulse generated using C_Q = 1.9 MHz and η_Q = 0 (black line) and applied at all values of η_Q or for a series of FAM-N pulses optimized using C_Q = 1.9 MHz and each specific η_Q value (gray line). Simulations were performed for a single [87]Rb ($I = 3/2$) nucleus at B_0 = 14.1 T, with $\omega_R/2\pi$ = 12.5 kHz and $\omega_1/2\pi$ = 114 kHz.

efficiency of the FAM-N pulse used above (generated using $\omega_1/2\pi$ = 114 kHz, $\omega_R/2\pi$ = 12.5 kHz, C_Q = 1.9 MHz, and η_Q = 0) changes as the value of η_Q for which it is applied varies. As shown by the black line, a small decrease in efficiency is observed as η_Q increases. If different FAM-N pulses are generated for each value of η_Q individually, this decrease is not as significant (as shown by the gray line), but the maximum single-quantum coherence generated still falls slightly with increasing η_Q. Table 1 compares the predicted efficiency of different FAM-N pulses (and the corresponding signal obtained
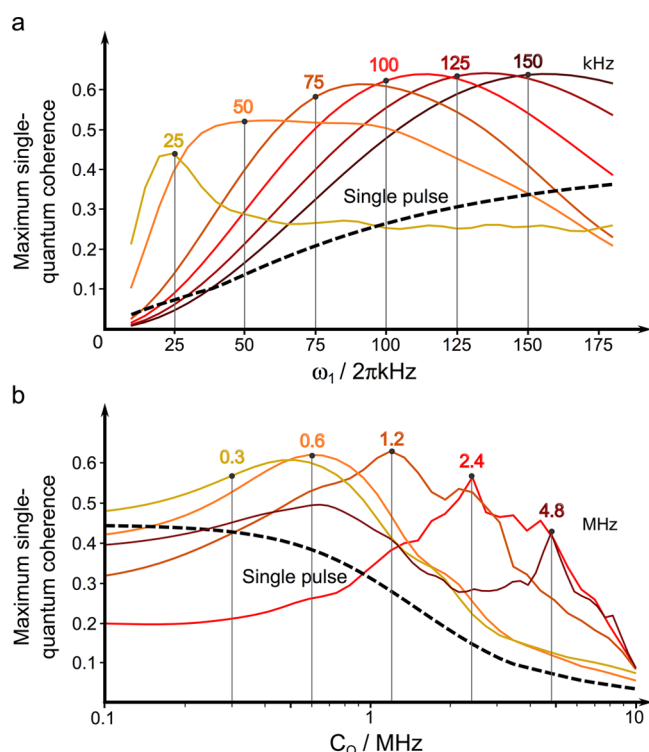
a

b

Figure 6. Plots showing how the maximum central-transition single-quantum coherence generated from unit triple-quantum coherence using a FAM-N pulse optimized at specific conditions varies with a change in (a) the inherent rf nutation rate, $\omega_1/2\pi$, and (b) the quadrupolar coupling constant, C_Q. Simulations were performed for a single ^{87}Rb ($I = 3/2$) nucleus at $B_0 = 14.1$ T, with $\eta_Q = 0$, $\omega_R/2\pi = 12.5$ kHz and in (a) $C_Q = 1.2$ MHz with $\omega_1/2\pi = 25$, 50, 75, 100, 125, and 150 kHz, and in (b) $\omega_1/2\pi = 114$ kHz with $C_Q = 0.3$, 0.6, 1.2, 2.4, and 4.8 MHz. The maximum efficiency obtained using a single pulse is shown by the black dotted line.

$\omega_R/2\pi = 12.5$ kHz, $C_Q = 1.9$ MHz, and $\eta_Q = 0$ varies when applied at different values of the rf field strength. It can be seen

that good performance is obtained over a reasonable range of nutation rates (i.e., 90% of the maximum performance is achieved over a range of 62 kHz). This suggests that small errors in the rf calibration measurement (or inaccuracies in any estimation) should have little impact on the efficiency of the FAM-N pulse. However, in cases where sufficient signal can be obtained, it is also possible to experimentally optimize the B_1 field strength used for the computer-generated FAM-N pulse to ensure maximum efficiency is obtained. Figure 6a demonstrates that this process is not vital, and for samples where this is not feasible in a reasonable time scale, an estimate of the inherent rf nutation rate is sufficient for successful implementation of FAM-N. One point to note from Figure 6a is that, although maximum efficiency at a rf nutation rate of, for example, 100 kHz is achieved by using the FAM-N pulse generated with that value of the rf as an initial input, the maximum efficiency of each FAM-N pulse is actually found when that same pulse is applied at slightly higher nutation rates (e.g., for the FAM-N pulse generated using $\omega_1/2\pi = 100$ kHz maximum efficiency for that specific pulse is found when $\omega_1/2\pi = 110$ kHz). This is most likely a result of the fact that small variations in rf nutation rate do not significantly affect the type/length of optimized pulse, but that the higher B_1 field strength applied can result in a slightly higher general conversion efficiency.

Figure 6b shows a plot considering how the efficiency of a specific FAM-N pulse (optimized at the C_Q value shown) varies as C_Q changes. Note the logarithmic scale on the x axis. Maximum enhancements are observed for C_Q values close to those for which the pulse was initially generated, but a significant enhancement is seen over the signal obtained using a single pulse over a range of C_Q values. This range is wider at lower values of C_Q (even accounting for the log scale), where the optimized FAM-N pulse consists of only a small number of individual pulses. Although the range of C_Q values where maximum efficiency is obtained drops as C_Q increases, the magnitude of the enhancement achieved at higher C_Q is greater. Figure 6b suggests that, although a prior estimate of the magnitude of the quadrupolar interaction is useful, significant
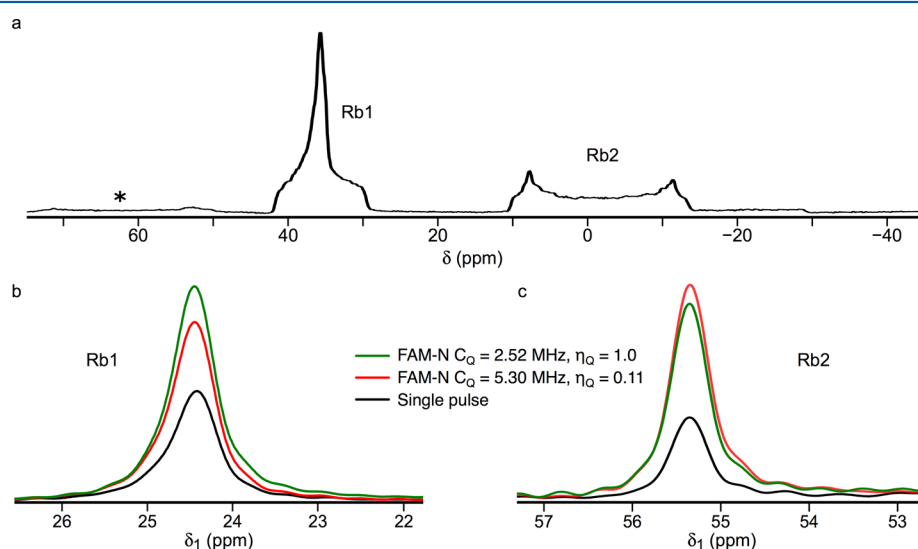

Figure 7. ^{87}Rb (14.1 T, 12.5 kHz) (a) MAS and (b) isotropic projections of triple-quantum MAS NMR spectra of Rb$_2$SO$_4$. In (b, c) spectra were acquired using the pulse sequence in Figure 1, using either a single pulse or FAM-N for the conversion of triple- to single-quantum coherences. Two FAM-N pulses were generated (i) using $C_Q = 2.52$ MHz and $\eta_Q = 1.0$ and (ii) using $C_Q = 5.3$ MHz and $\eta_Q = 0.11$, each with $\omega_1/2\pi = 123$ kHz. For full details of the experimental parameters, see the Supporting Information.

enhancements may still be achieved for different C_Q values. The presence of multiple sites with differing C_Q values within a sample presents a challenge for any sensitivity enhancement technique but is a common situation in reality. Figure 7 shows both a MAS spectrum and isotropic projections obtained from ^{87}Rb two-dimensional triple-quantum MAS NMR experiments on Rb_2SO_4, acquired using the phase-modulated split-t_1 shifted-echo pulse sequence shown in Figure 1. The conversion of triple- to single-quantum coherences has been carried out either with a single (high-power) pulse or with FAM-N. There are two distinct Rb sites in Rb_2SO_4 (as can be seen in the MAS spectrum, shown in Figure 7a), with C_Q values of ~2.5 and ~5.3 MHz, respectively.[26] Two FAM-N pulses were used for conversion: one generated from an optimization using C_Q = 2.52 MHz and η_Q = 1.0 and a second using C_Q = 5.30 MHz and η_Q = 0.11. In both cases, values of $\omega_1/2\pi$ = 123 kHz and $\omega_R/2\pi$ = 12.5 kHz were used in the computer-based optimization. For Rb1 (C_Q = 2.52 MHz), as shown in Figure 7b, the maximum enhancement (of ~105% over a single pulse) is seen with the pulse generated using that C_Q value, but only 12% of the signal is lost when the alternative FAM-N conversion pulse is used. A similar result is also observed for Rb2 (Figure 7c), with maximum enhancement obtained using the FAM-N pulse generated from an optimization using C_Q = 5.30 MHz, and the signal enhancement dropping from 160% to 135% (both compared to the signal obtained using a single pulse) when the FAM-N pulse is changed.

■ CONCLUSIONS

We have demonstrated an effective and high-throughput approach for the generation of amplitude-modulated pulses to enhance the efficiency of the conversion of triple- to single-quantum coherences, a transfer used in many NMR experiments for quadrupolar nuclei, including the popular MQMAS technique. The optimization is easy to perform, using SIMPSON and MATLAB packages, and results in very efficient pulses that can be used directly in experiment. The efficiency of the pulses reported here exceeds that of multiple-pulse schemes based on FAM-II reported previously in the literature,[13,18] most likely owing to the fact that earlier optimization approaches used constraints on the lengths of some or all of the pulses. Most significant signal enhancements are obtained when good estimates of the inherent rf nutation rate and the magnitude of the quadrupolar coupling are used as initial input to the computer-based optimization process, but the pulses appear reasonably robust to variations in either of those parameters, producing significant enhancements over the signal obtained using a single pulse for conversion, and also improved efficiency over more commonly used approaches such as FAM-I, FAM-II, and SPAM. A performance similar to that of DFS is observed, although the ease of implementation (i.e., little or no experimental optimization) of FAM-N offers a significant advantage, particularly for systems where sensitivity is limited (e.g., low-γ nuclei, small sample volumes, low natural abundance, or low element density). If sufficient signal can be observed on a reasonable time scale, it is possible to optimize the B_1 field strength at which the pulse is applied experimentally to ensure maximum signal enhancement. This approach offers great potential to routinely improve MQMAS and MQMAS-based correlation experiments on a wide range of materials, opening up (particularly in combination with high-field measurements) the study of nuclei and systems that have perhaps previously been deemed "too difficult". Future work

will focus on extending this approach to improve other coherence transfer processes (e.g., single- to triple-quantum coherence, five- to single-quantum coherence, etc.) and upon application to more challenging cases, such as ^{25}Mg and ^{67}Zn NMR (where the low γ will result in very low ω_1) or samples with low content of a particular element. Furthermore, similar approaches have been used for population transfers[27] and transfer from 0 to −1 coherences[28] and high-throughput optimizations using our approach may offer further sensitivity enhancements in these cases.

■ ASSOCIATED CONTENT

ⓢ Supporting Information
Information on the optimization procedure, comparison of conversion schemes, and experimental details for the ^{87}Rb experiments on $RbNO_3$ and Rb_2SO_4 and predicted efficiency (in simulation) of FAM-N pulses. Examples of the MATLAB and results text files are also provided (full copies of any programs are available from the authors on request). This material is available free of charge via the Internet at http://pubs.acs.org.

■ AUTHOR INFORMATION

Corresponding Author
*S. E. Ashbrook. E-mail: sema@st-andrews.ac.uk.
Notes
The authors declare no competing financial interest.

■ ACKNOWLEDGMENTS

■ REFERENCES

(1) Apperley, D. C.; Harris, R. K.; Hodgkinson, P. *Solid State NMR Basic Principles and Practice*; Momentum Press: New York, 2012.
(2) Andrew, E. R. Magic Angle Spinning. *eMagRes.*; Wiley: New York, 2007; DOI 10.1002/9780470034590.emrstm0283.
(3) *NMR of Quadrupolar Nuclei in Solid Materials*; Wasylishen, R. E., Ashbrook, S. E., Wimperis, S., Eds.; John Wiley & Sons, Ltd.: Chichester, U.K., 2012.
(4) Samoson, A.; Lippmaa, E.; Pines, A. High Resolution Solid-State N.M.R. *Mol. Phys.* **1988**, *65*, 1013−1018.
(5) Llor, A.; Virlet. Towards High-Resolution NMR of More Nuclei in Solids − Sample Spinning with Time-Dependent Spinner Axis Angle. *J. Chem. Phys. Lett.* **1988**, *152*, 248−253.
(6) Frydman, L.; Harwood, J. S. Isotropic Spectra of Half-Integer Quadrupolar Spins from Bidimensional Magic-Angle-Spinning NMR. *J. Am. Chem. Soc.* **1995**, *117*, 5367−5368.
(7) (a) Goldbourt, A.; Madu, P. K. Multiple-quantum magic-angle spinning: High-resolution solid-state NMR of half-integer spin quadrupolar nuclei. *Annu. Rep. NMR Spectrosc.* **2005**, *54*, 81−153. (b) Rocha, J.; Fernandez, C. Progress in multiple-quantum magic-angle spinning NMR spectroscopy. *New Techniques in Solid-State NMR* **2005**, *246*, 141−194. (c) Johnston, K. E.; Tang, C. C.; Parker, J. E.; Knight, K. S.; Lightfoot, P.; Ashbrook, S. E. The Polar Phase of NaNbO$_3$: A Combined Study by Powder Diffraction, Solid-State NMR, and First-Principles Calculations. *J. Am. Chem. Soc.* **2010**, *123*, 8732−8746. (d) Buannic, L.; Blanc, F.; Hung, I.; Gan, Z. H.; Grey, C. P. Probing the local structures and protonic conduction pathways in scandium substituted BaZrO$_3$ by multinuclear solid-state NMR spectroscopy. *J. Mater. Chem.* **2010**, *30*, 6322−6332. (e) Griffin, J. M.; Ashbrook, S. E. Solid-State NMR of High-Pressure Silicates in the Earth's Mantle. *Annu. Rep. NMR Spectrosc.* **2013**, *79*, 241−332. (f) Florian, P.; Veron, E.; Green, T. F. G.; Yates, J. R.; Massiot, D.

Elucidation of the Al/Si Ordering in Gehlenite $Ca_2Al_2SiO_7$ by Combined Si-29 and Al-27 NMR Spectroscopy/Quantum Chemical Calculations. *Chem. Mater.* **2012**, *24*, 4068−4079. (g) Griffin, J. M.; Clark, L.; Seymour, V. R.; Aldous, D. W.; Dawson, D. M.; Iuga, D.; Morris, R. E.; Ashbrook, S. E. Ionothermal ^{17}O Enrichment of Oxides using Microlitre Quantities of Labelled Water. *Chem. Sci.* **2012**, *3*, 2293−2300. (h) Amri, M.; Ashbrook, S. E.; Dawson, D. M.; Griffin, J. M.; Walton, R. I.; Wimperis, S. A Multinuclear Solid-State NMR Study of Templated and Calcined Chabazite-Type GaPO-34. *J. Phys. Chem. C* **2012**, *116*, 15048−15957. (i) Haouas, M.; Martineau, C.; Taulelle, F. Quadrupolar NMR of Nanoporous Materials. *eMagRes.*; Wiley: New York, 2011; DOI 10.1002/9780470034590.emrstm1216. (j) Du, L.-S.; Stebbins, J. F. Network Connectivity in Aluminoborosilicate Glasses: a High-Resolution ^{11}B, ^{27}Al and ^{17}O NMR Study. *J. Non-Cryst. Solids* **2005**, *351*, 3508−3520. (k) Kroeker, S. Nuclear Waste Glasses: Insights from Solid-State NMR. *eMagRes.*; Wiley: New York, 2011; DOI 10.1002/9780470034590.emrstm1223.

(8) Gan, Z. Isotropic NMR Spectra of Half-Integer Quadrupolar Nuclei using Satellite Transitions and Magic-Angle Spinning. *J. Am. Chem. Soc.* **2000**, *122*, 3242−3243.

(9) Ashbrook, S. E.; Wimperis, S. High-Resolution NMR of Quadrupolar Nuclei in Solids: the Satellite-Transition Magic Angle Spinning (STMAS) Experiment. *Prog. Nucl. Magn. Reson. Spectrosc.* **2004**, *45*, 53−108.

(10) (a) Ashbrook, S. E.; Berry, A. J.; Hibberson, W. O.; Steuernagel, S.; Wimperis, S. High-Resolution ^{17}O NMR Spectroscopy of Wadsleyite (β-Mg_2SiO_4). *J. Am. Chem. Soc.* **2003**, *125*, 11824−11825. (b) Lapina, O. B.; Khabibulin, D. F.; Romanenko, K. V.; Gan, Z.; Zuev, M. G.; Krasilnkov, V. N.; Fedrov, V. E. ^{93}Nb NMR Chemical Shift Scale for Niobia Systems. *Solid State Nucl. Magn. Reson.* **2005**, *28*, 204−224. (c) Antonijevic, S.; Ashbrook, S. E.; Biedesek, S.; Walton, R. I.; Wimperis, S.; Yang, H. X. Dynamics on the Microsecond Timescale in Microporous Aluminophosphate AlPO-14 as Evidenced by ^{27}Al MQMAS and STMAS NMR Spectroscopy. *J. Am. Chem. Soc.* **2006**, *128*, 8054−8062. (d) Trebosc, J.; Amoureux, J. P.; Gan, Z. Comparison of High-Resolution Solid-State NMR MQMAS and STMAS Methods for Half-Integer Quadrupolar Nuclei. *Solid State Nucl. Magn. Reson.* **2007**, *31*, 1−9. (e) Ashbrook, S. E.; Berry, A. J.; Frost, D. J.; Gregorovic, A.; Pickard, C. J.; Readman, J. E.; Wimperis, S. ^{17}O and ^{29}Si NMR Parameters of $MgSiO_3$Phases from High-Resolution Soild-State NMR Spectroscopy and First-Principles Calculations. *J. Am. Chem. Soc.* **2007**, *129*, 13213−13224. (f) Griffin, J. M.; Wimperis, S.; Berry, A. J.; Pickard, C. J.; Ashbrook, S. E. Solid-State ^{17}O NMR Spectroscopy of Hydrous Magnesium Silicates: Evidence for Proton Dynamics. *J. Phys. Chem. C* **2009**, *113*, 465−471.

(11) Kentgens, A. P. M.; Verhagen, R. Advantages of Double Frequency Sweeps in Static, MAS and MQMAS NMR of Spin I = 3/2 Nuclei. *Chem. Phys. Lett.* **1999**, *300*, 435−443.

(12) (a) Madhu, P. K.; Goldbourt, A.; Frydman, L.; Vega, S. Sensitivity Engancement of the MQMAS NMR Experiment by Fast Amplitude Modulation of the Pulses. *Chem. Phys. Lett.* **1999**, *307*, 41−47. (b) Madhu, P. K.; Goldbourt, A.; Frydman, L.; Vega, S. Fast Radio-Frequency Amplitude Modulation in Multiple-Quantum Magic-Angle-Spinning Nuclear Magnetic Resonance: Theory and Experiments. *J. Chem. Phys.* **2000**, *112*, 2377−2391.

(13) Goldbourt, A.; Madhu, P. K.; Vega, S. Enhanced Conversion of Triple to Single-Quantum Coherence in the Triple-Quantum MAS NMR Spectroscopy of Spin-5/2 Nuclei. *Chem. Phys. Lett.* **2000**, *320*, 448−456.

(14) Gan, Z.; Kwak, H. T. Enhancing MQMAS Sensitivity Using Signals from Multiple Coherence Transfer Pathways. *J. Magn. Reson.* **2004**, *168*, 346−351.

(15) Amoureux, J. P.; Delevoye, L.; Steuernagel, S.; Gan, Z.; Ganapathy, S.; Montagne, L. Increasing the Sensitivity of 2D High-Resolution NMR Methods Applied to Quadrupolar Nuclei. *J. Magn. Reson.* **2005**, *172*, 268−278.

(16) Siegel, R.; Nakashima, T. T.; Wasylishen, R. E. Sensitivity Enhancement of MQMAS NMR Spectra of Spin 3/2 Nuclei using Hyperbolic Secant Pulses. *Chem. Phys. Lett.* **2005**, *403*, 353−358.

(17) Ball, T. J.; Wimperis, S. Use of SPAM and FAM Pulses in High-Resolution MAS NMR Spectroscopy of Quadrupolar Nuclei. *J. Magn. Reson.* **2007**, *187*, 343−351.

(18) Morais, C. M.; Lopes, M.; Fernandez, C.; Rocha, J. Assessing the Potential of Fast Amplitude Modulation Pulses for Improving Triple-Quantum Magic Angle Spinning NMR Spectra of Half-Integer Quadrupolar Nuclei. *Magn. Reson. Chem.* **2003**, *41*, 679−688.

(19) Iuga, D.; Schäfer, H.; Verhagen, R.; Kentgens, A. P. M. Population and Coherence Transfer Induced by Double Frequency Sweeps in Half-Integer Quadrupolar Systems. *J. Magn. Reson.* **2000**, *147*, 192−209.

(20) Bak, M.; Rasmussen, J.; Nielsen, N. SIMPSON: A General Simulation Program for Solid-State NMR Spectroscopy. *J. Magn. Reson.* **2000**, *147*, 296−330.

(21) *MATLAB* Release 2011b; The MathWorks, Inc.: Natick, MA, United States.

(22) MacKenzie, K. J. D.; Smith, M. E. *Multinuclear Solid-State NMR of Inorganic Materials*; Pergamon Press: Oxford, U.K., 2002.

(23) Brown, S. P.; Wimperis, S. Two-Dimensional Multiple-Quantum MAS NMR of Quadrupolar Nuclei. Acquisition of the Whole Echo. *J. Magn. Reson.* **1997**, *124*, 279−285.

(24) Pike, K. J.; Malde, R. P.; Ashbrook, S. E.; McManus, J.; Wimperis, S. Multiple-Quantum MAS NMR of Quadrupolar Nuclei. Do Five-, Seven- and Nine-Quantum Experiments Yield Higher Resolution than the Three-Quantum Experiment? *Solid State Nucl. Magn. Reson.* **2000**, *16*, 203−215.

(25) Massiot, D.; Touzo, B.; Trumeau, J. P.; Virlet, J.; Florian, P.; Grandinetti, P. J. Two-Dimensional Magic-Angle Spinning Isotropic Reconstruction Sequences for Quadrupolar Nuclei. *Solid State Nucl. Magn. Reson.* **1996**, *6*, 73−83.

(26) Vosegaard, T.; Skibsted, J.; Blidsoe, H.; Jakobsen, H. J. Quadrupole Coupling and Anisotropic Shielding from Single-Crystal NMR of the Central Transition for Quadrupolar Nuclei. ^{87}Rb NMR of $RbClO_4$ and Rb_2SO_4. *J. Magn. Reson. A* **1996**, *122*, 111−119.

(27) (a) Perras, F. A.; Viger-Gravel, J.; Burgess, K. M. N.; Bryce, D. Signal Enhancement in Solid-State NMR of Quadrupolar Nuclei. *Solid State Nucl. Magn. Reson.* **2013**, *51−52*, 1−15. (b) Siegel, R.; Nakashima, T. T.; Wasylishen, R. E. Sensitivity Enhancement of NMR Spectra of Half-Integer Quadrupolar Nuclei in the Solid State via Population Transfer. *Concepts Magn. Reson. A* **2005**, *26A*, 47−61.

(28) Carnevale, D.; Bodenhausen, G. Composite Pulses for Efficient Excitation of Half-Integer Quadrupolar Nuclei in NMR of Static and Spinning Solid Samples. *Chem. Phys. Lett.* **2012**, *530*, 120−125.